

EFFECT OF THE BAR DIAMETER ON THE LOAD RESPONSE OF GFRP-CONCRETE PULL-OUT TESTS

Xudong Zhao, Case Western Reserve University, USA, xxz435@case.edu

Mohammad Minhajur Rahman, Case Western Reserve University, USA, mxr653@case.edu

Tommaso D'Antino, Politecnico di Milano, Italy, tommaso.dantino@polimi.it

Francesco Focacci, eCampus University, Italy, francesco.focacci@uniecampus.it

Christian Carloni, Case Western Reserve University, USA, cxc966@case.edu

ABSTRACT

This study focuses on the effect of the bar diameter of glass fiber-reinforced polymer (GFRP) bars on their bond with concrete using pull-out tests. The investigation involves three nominal bar diameters: 6 mm, 12 mm, and 20 mm and several bonded lengths. Within this study, the pull-out test results for both the 6 mm and 20 mm bars are presented for the first time, whereas the findings for the 12 mm bars were previously reported in a paper by the authors, where the effect of the bonded length on the experimental response was assessed. The influence of the bonded length on the bond strength for different diameters is discussed. Different bonded lengths are considered for each bar diameter, and the load responses are discussed.

KEYWORDS

Glass fiber-reinforced polymer (GFRP), Bond, Bar diameter, Pull-out test

INTRODUCTION

Concrete reinforcement steel bars are being increasingly substituted with fiber-reinforced polymer (FRP) bars due to the numerous advantages of FRP bars, such as their cost-effectiveness, high tensile strength, resistance to corrosion, lightweight, high durability, and electro-magnetic transparency (C. Arya et al., 2012; El-Hacha et al., 1993; Fib, 2007). The market offers a wide range of options for GFRP bars, and extensive research has been conducted on their mechanical behavior as internal reinforcement for concrete structures. This includes investigations into different bar diameters (Achillides & Pilakoutas, 2004; Baena et al., 2009; El Refai et al., 2015; Sayed Ahmad et al., 2011), fiber types (Achillides & Pilakoutas, 2004; Baena et al., 2009), and surface treatments (Achillides & Pilakoutas, 2004; Arias et al., 2012; Shen et al., 2016). Among these factors, the bar diameter holds significant importance as it influences the bond behavior between GFRP bars and concrete.

To investigate the bond between FRP bars and concrete, concentric pull-out tests have been used by many researchers. Existing guidelines for pull-out tests such as ASTM D7913 (ASTM D30, 2020), ACI 440.3R-12 (ACI 440, 2012), and CSA S806-12 (CSA, 2021) suggest a bonded length, ℓ , that is either 4 or 5 times the nominal diameter d_b of the bar. However, it is important to note that these test guidelines were originally intended for laboratory tests aimed at studying the effect of bar size and the type of FRP, rather than establishing a design bond strength or development length. Thus, longer bonded length such as $10d_b$, $20d_b$, and $40d_b$ were considered in this study. According to ASTM D7913 (ASTM D30, 2020), the bond stress, τ , is defined as the applied load, P , divided by the interface area between the bar and concrete, i.e., $\tau = P / \pi d_b \ell$. Additionally, it defines bond strength as the maximum bond stress, which corresponds to the peak applied load. It is important to note, however, that this terminology can be misleading because the bond strength should be the maximum shear stress developed at the bar-concrete interface, rather than its average value. Therefore, in this paper, the term *average bond strength* will be used to define the bond stress at the bond interface at peak load. An *average bond strength* equation with multi factors can be analytically derived from the experimental results. The derivation of such an equation from experimental data allows for a more comprehensive understanding of the bond between the FRP bar and concrete and provides a useful

tool for predicting the development length in practical applications (Huang et al., 2020; Okelo & Yuan, 2004; Tighiouart et al., 1998).

The influence of bar diameter on the mechanical behavior of FRP bars has been extensively explored in the literature. The majority of studies indicate that increasing the bar diameter is associated with a decrease in the average bond strength (Achillides & Pilakoutas, 2004; Baena et al., 2009; Hu et al., 2022). However, there are some contradictory findings reported in certain studies (Rolland et al., 2018; Wei et al., 2019). In general, as the bar diameter increases, the bar's tensile strength tends to decrease, while the elastic modulus remains relatively constant (Sireg Geotech S r. l., 2017). This behavior can be attributed to challenges in the pultrusion process and the uneven distribution of axial stresses across the bar cross-section in larger diameter bars. A recent study (Junyan et al., 2021) investigating the bond between basalt FRP (BFRP) bars and coral reef and sand concrete revealed that smaller bar diameters and shorter bond lengths tend to result in a higher likelihood of pull-out failure as the predominant failure mode. In the case of BFRP bars, another study indicated that the bar diameter has no significant effect on certain physical characteristics of the bar (Ali et al., 2020). Overall, the effect of bar diameter on bond behavior is complex and can vary depending on the specific conditions and materials involved.

MATERIAL PROPERTIES AND SPECIMEN PREPARATION

This study focused on investigating three different diameters of the same type of glass FRP (GFRP) bar, denoted as M6, M12, and M20, which correspond to a nominal diameter d_b equal to 6 mm, 12 mm, and 20 mm. The actual diameters of the bars were 6.1 mm, 12.7 mm, and 20.5 mm, and were determined using the immersion method (ISO, 2015) and provided by the manufacturer (Sireg Geotech S r. l., 2017). The bars had a cross-sectional area of 29.1 mm², 127.0 mm², and 330.1 mm² respectively. All the bars had the surface coated with sand. Additionally, the bars were wrapped with a spirally wound carbon yarn, with spacing of 25 mm, 30 mm, and 28 mm for the M6, M12, and M20 bars (Figure 1a). The properties of the GFRP bars, according to the manufacturer's data sheet (Sireg Geotech S r. l., 2017), are listed in Table 1,

Table 1 – Properties of GFRP bars from manufacturer (Sireg Geotech S r. l., 2017)

Bar type	Nominal bar diameter (mm)	Actual bar diameter (mm)	Cross-sectional area (mm ²)	Ultimate tensile load (kN)	Ultimate tensile strength (MPa)
M6	6	6.1	29.1	30	1000
M12	12	12.7	127.0	120	950
M20	20	20.5	330.1	295	900

Tensile tests were conducted on both M6 and M20 bars to confirm that steel hollow cylinders glued at the ends of the bars were adequate to grip the bars by means of the testing machine jaws. This paper used the same tensile test set-up and method as the previous work by the authors for the M12 bar (Zhao et al., 2022). For the M6 and M20 bars, steel hollow cylinders with lengths of $L_{cyl}=152$ mm and 304 mm, respectively, were used. The free length, L_f , of the tensile test specimens for both bars was set to 304 mm. Similar to the tensile tests conducted on the M12 bars described in (Zhao et al., 2022), the steel cylinders were internally threaded to enhance the bond, using epoxy resin to securely connect the bar to the cylinder.

The tensile tests were conducted using a stroke control method at a rate of 1.5 mm/min, according to (ASTM International, 2016). Two M6 bars were tested until tensile failure occurred. The average peak load during the tensile tests was measured as 37.6 kN, resulting in a corresponding tensile strength of 1291 MPa. The test results are plotted in Figure 1b in terms of applied load against the machine stroke. M20 bars were loaded up to 200 kN due to the maximum capacity limitation of the testing machine, which was 250 kN. The results obtained from the tensile tests on the M20 bars provided confirmation that the steel cylinder with a length of 304 mm was sufficient to conduct pull-out tests up to at least 200 kN. The results of the tensile tests on M12 bars are reported in Figure 1b for comparison. It should be noted that, although the free length L_f and the length of the cylinders L_{cyl}

were shorter than prescribed in (ASTM D30, 2021)), the setup of the tensile tests allowed to attain the tensile strength of the bars considered in this work and the cylinders proved to be adequate for gripping the bars during the pull-out tests.

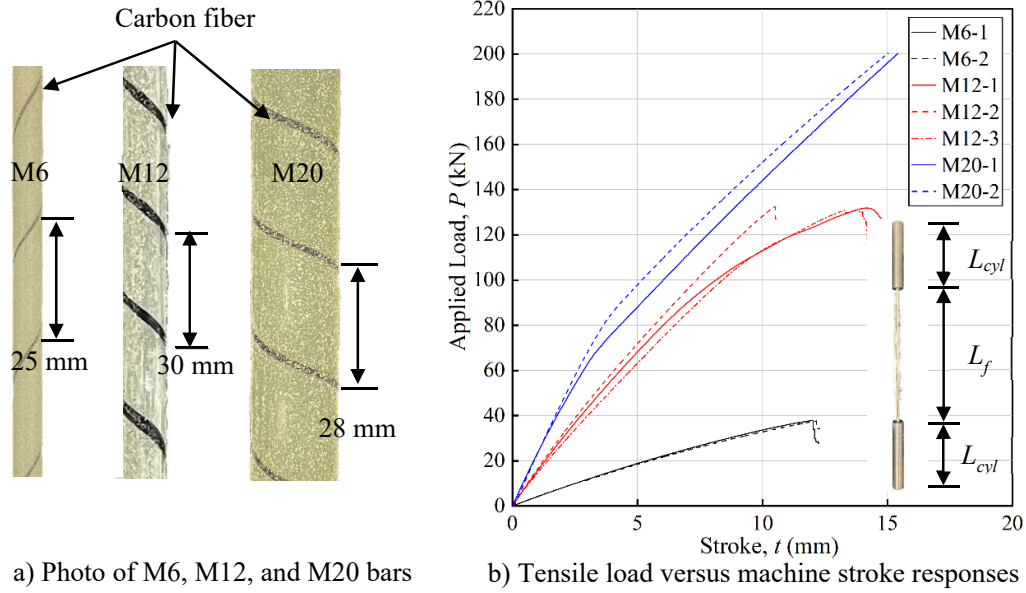


Figure 1: GFRP bar characteristics and tensile tests of M6, M12, and M20 GFRP bars

A single concrete batch was used to cast both the pull-out specimens for the M6 and M20 bars, and the concrete cylinders for material characterization. The concrete mixture was proportioned based on weight, with the following mix ratios: 1 part water, 2.6 parts cement, 10.3 parts fine aggregate, and 10.5 parts coarse aggregate. The maximum aggregate size used in the mixture was 12 mm. To assess the workability of the fresh concrete, a slump test was conducted in accordance with ASTM C09 (ASTM C09, 2020b). The measured slump value obtained at the beginning of casting was 152.4 mm. The average compressive strength (f'_c) of concrete was determined following the procedure outlined in ASTM C39 (ASTM C09, 2020a). At 28 days, f'_c was equal to 41.6 MPa with coefficient of variation (CoV) of 0.029. The mechanical properties of concrete used for the M12 specimens are reported in (Zhao et al., 2022).

TEST SETUP

The pull-out test setup utilized in this study for the M6 and M20 bar specimens was the same as the one previously designed by the authors for the M12 bars (Figure 2). Detailed information about the setup can be found in (Zhao et al., 2022). In summary, the experimental setup involved one end of the GFRP bar being pulled by the machine head, while a frame consisting of steel plates and steel bars restrained the concrete cylinder. The GFRP bar extended beyond the free end by 50 mm for most of the specimens. Some specimens were obtained by removing the bottom part of the concrete cylinder to obtain a specific bonded length. The pull-out specimens in this study were labeled using the notation Y-X-Zc. Y represented the nominal diameter of the GFRP bar being tested. X denoted the bonded length ℓ , expressed as a multiple of the bar diameter. The letter Z was assigned as a specimen number to distinguish between specimens with the same diameter of the bar and bonded length. c was used in the specimen name after Z for those specimens that were cut to obtain the desired bonded length and therefore did not have the protruding part of the bar at the free end. Three linear variable displacement transformers (LVDTs), named TL₁, TL₂, and TL₃, were installed on bare portions the bar, positioned 130 mm away from the top surface of the concrete cylinder. The average of the

readings from these three LVDTs was used to calculate the slip at the loaded end (g). Additionally, two LVDTs, named BL_1 and BL_2 , were installed at the bottom end of the concrete cylinder to measure the slip, δ , at the free end. An extensometer was installed on some selected specimens to measure the elongation of the free portion of the GFRP bar during the pull-out test.

The pull-out tests were carried out using different control modes depending on the presence of bottom LVDTs. For specimens without LVDTs BL_1 and BL_2 , the tests were conducted in stroke control. For specimens equipped with LVDTs BL_1 and BL_2 , the tests were conducted in using the average of TL_1 , TL_2 , and TL_3 LVDTs. The initial loading rate (stroke control) was set at 1.3 mm/min. After reaching the first peak load and observing a descending load response, the loading rate was doubled. Once the free end part of the bar began slipping into the concrete cylinder, the loading rate was tripled. For LVDT controlled tests, the initial rate was 0.88 mm/min and it was increased with the same protocol as for the stroked controlled specimens.

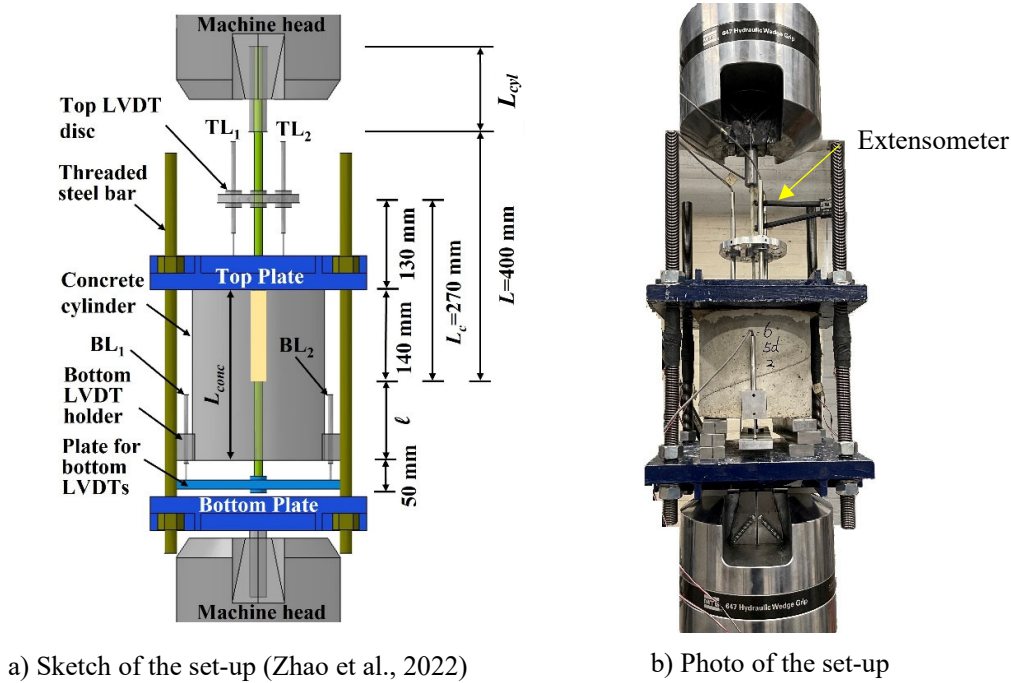


Figure 2: Pull-out test set-up

TEST RESULTS AND DISCUSSION

Effect of bar diameter on GFRP bar elastic modulus

During the tensile test on the M20 bar, an extensometer with a gauge length of 50 mm was installed to measure the bar's axial strain. However, for the M6 bars, the extensometer was not used during the tensile tests. Nevertheless, for three pull-out test specimens with M6 bars, the extensometer was installed between the disc (attached to the bar and used to mount TL_1 , TL_2 , and TL_3 LVDTs) and the steel hollow cylinder used for gripping the bar (Figure 2). The elastic modulus (E_b) values were obtained from the extensometer measurement and reported in Table 2. The data for the M12 bar was obtained from a previous study (Zhao et al., 2022). The results indicate that the elastic modulus (E_b) increases as the bar diameter decreases. This trend can be attributed to the non-uniform distribution of axial stress across the bar cross-section, as discussed in (Zhao et al., 2022).

Applied load P versus machine stroke t and loaded end slip g responses.

Figure 3a, b, and c present the load responses of the specimens with M6, M12, and M20 bars in terms of applied load (P) versus machine stroke (t). Figure 3a illustrates the load responses of M6 bar specimens with various bonded lengths, namely $\ell = 30$ mm, 60 mm, 120 mm, and 240 mm. These responses exhibit an initial linear portion followed by a brief nonlinear phase before reaching the peak

load. Subsequently, the descending part of the responses shows oscillations that become more prominent as ℓ increases. It can be observed that the amplitude of the oscillations was related to the bonded length, with longer bonded lengths exhibiting more significant oscillations. It is worth noting that the frequency of oscillation remains similar regardless of the bonded length. This observation aligns with the findings in (Zhao et al., 2022), which suggest that the presence of carbon fiber yarn contributes to the occurrence of oscillations. The average interval between oscillations was approximately 20 mm in stroke. For specific specimens (6-5d-2, 6-5d-3, 6-10d-1, 6-10d-2, and 6-20d-2), the tests were conducted in LVDT control. The presence of the aluminum plate to mount LVDTs BL₁ and BL₂ limited the duration of the test, and it was stopped when the stroke value reached approximately 25 mm to prevent contact between the aluminum plate and the bottom surface of the concrete cylinder. For the remaining specimens tested in stroke control, the tests continued until the free end of the bar slipped inside the concrete cylinder by 10 mm for specimens with bonded lengths of 30 mm and 60 mm, and by 30 mm for specimens with a bonded length of 120 mm. In the case of specimens with a bonded length of 240 mm, the GFRP bar experienced tension failure. The average applied load at fiber rupture was found to be 37.57 kN, which is consistent with the results obtained from the tensile tests conducted on M6 bars.

Table 2 – Elastic modulus of the GFRP bars.

GFRP bar	Elastic modulus E_b (GPa)	Elastic modulus (GPa)	
		Average	CoV
M6	52.6	51.4	0.024
	50.1		
	51.5		
M12	51.9	49.7	0.039
	49.2		
	48.1		
M20	49.1	48.0	0.034
	46.8		

Figure 3b illustrates the load responses of M20 bar specimens. The specimens had bonded lengths of 95 mm ($5d_b$), 152 mm ($8d_b$), and 240 mm ($12d_b$). Like the M6 specimens, the load responses initially follow a linear trend and then exhibit a non-linear branch before reaching the peak load. After the peak, the applied load decreased while showing oscillations. It was observed that the specimens without the protruding part at the free end (20-5d-5c, 20-5d-6c, 20-5d-7c, 20-5d-8c, 20-8d-5c, 20-12d-4c, and 20-12d-5c) had lower peak loads compared to specimens with the protruding part and the same bonded length. This observation is consistent with the findings from pull-out tests on M12 bars (Zhao et al., 2022). The protruding part can be considered as an anchorage system at the free end, which enhances the load transfer. During the pull-out test, as the applied load increases, the stress transfer zone propagates from the loaded end to the free end. The force in the protruding part is always zero, whereas when the free end starts to slip a gradient of the axial force in the bar occurs near the free end inside the concrete. This axial force is associated with the interfacial shear stress corresponding to the slip. The force in the bar corresponds to a decrease of the diameter of the bar (Poisson's effect) from the free end inward, which results in a funnel shape of the bar near the protruding part. Consequently, a certain amount of energy is required to pull in the protruding part of the bar at the free end. For specimens 20-5d-2, 20-5d-3, 20-10d-3, and 20-12d-3, the average of TL₁, TL₂, and TL₃ LVDTs was used for control, and LVDTs BL₁ and BL₂ were installed at the bottom end of the concrete cylinder to measure the free end slip of the bar. These tests were stopped when the stroke value reached approximately 25 mm. For the remaining specimens with M20 bars, the tests were stopped when the protruding part of the bar slipped inside the concrete cylinder.

Figure 3c illustrates the load responses of M12 bar specimens, which can be found in the previous paper by the authors (Zhao et al., 2022). The load responses exhibited a similar behavior to those of

the specimens with M6 and M20 bars, and they contributed to the understanding of the effect of bar diameter on the bond behavior of GFRP bars.

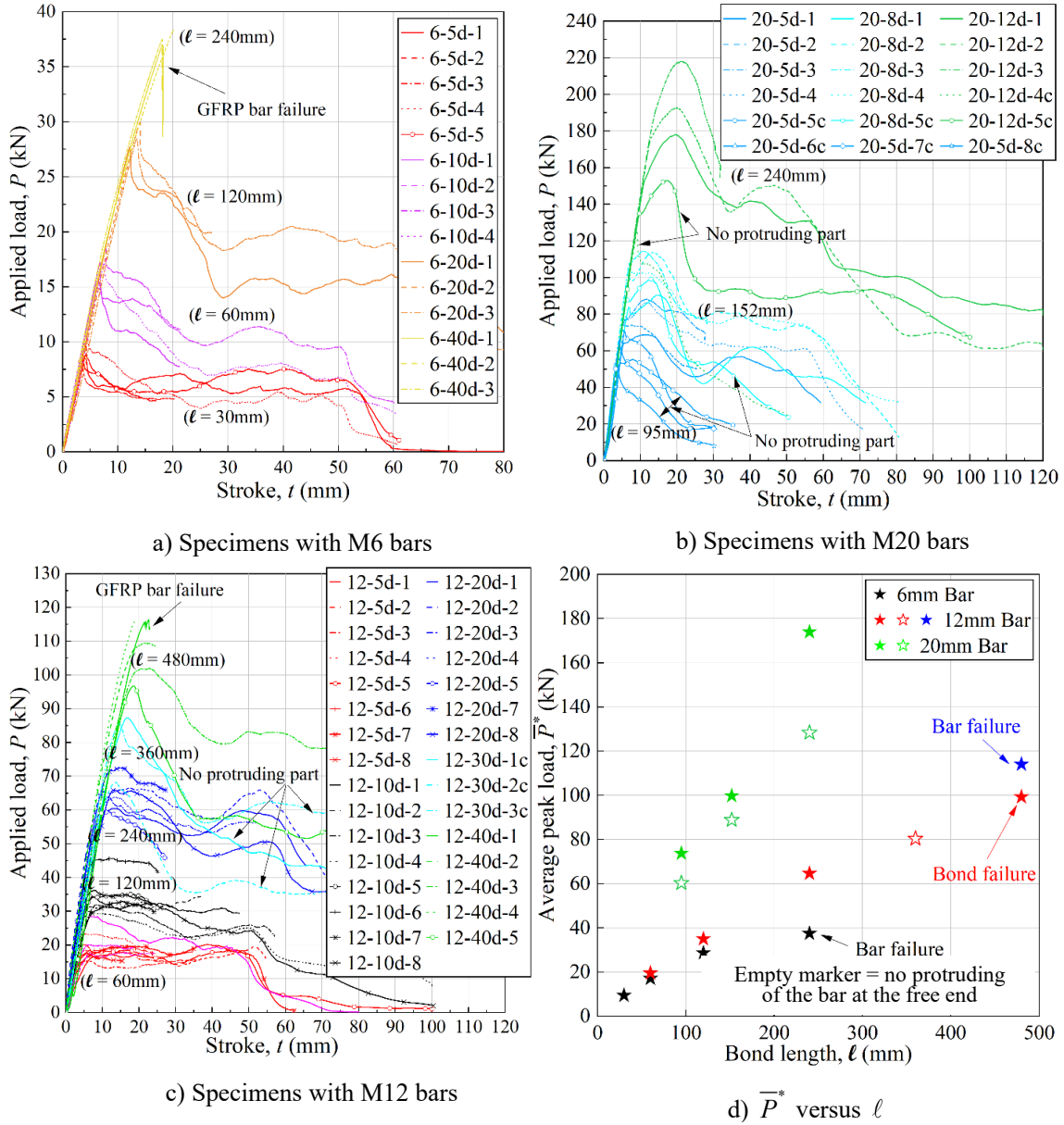


Figure 3: Applied load P versus machine stroke t responses and average peak load \bar{P}^* versus bonded length ℓ

The average peak load \bar{P} for each bar diameter and bond length was calculated and plotted against the bond length in Figure 3d for comparison. As previously mentioned, the specimens without a protruding part exhibited lower average peak loads compared to the specimens with a protruding part. An empty marker was used to represent the average peak load of specimens without the protruding part. Furthermore, it is evident that larger bar diameters resulted in higher average peak loads due to the larger interaction surface area between the bar and the surrounding concrete. Comparing the M6 bar specimens to the M12 bar specimens with the same bonded length, the average peak load of the M6 bar specimens was slightly lower but very close to that of the M12 bar specimens. The detailed effects of bar diameter on the bond behavior are discussed in the following Section.

Figure 4a shows the applied load versus the three separate readings of the LVDTs TL₁, TL₂, and TL₃ for the representative specimen 6-10d-3. The response of the three top LVDTs (TL₁, TL₂, and TL₃) is consistent, indicating the reliability of the measurements. These LVDTs were installed on the GFRP bar at a distance $L_c=270$ mm from the beginning of the bonded area (Figure 2a). The loaded end slip (g) is calculated by subtracting the elongation of the portion of the bar corresponding to L_c from the average of the top LVDT readings, i.e., $g = \xi - L_c \varepsilon_b$, where ξ is the average of the three top LVDTs and ε_b is the strain in the GFRP bar. The deformation of the concrete cylinder and top plate were neglected due to their negligible values compared to the bar elongation. Figure 4b presents the applied load (P) versus loaded end slip (g) for representative specimens with different GFRP bar diameters. It can be observed that the initial slope of the response increases as the bar diameter increases, which was expected.

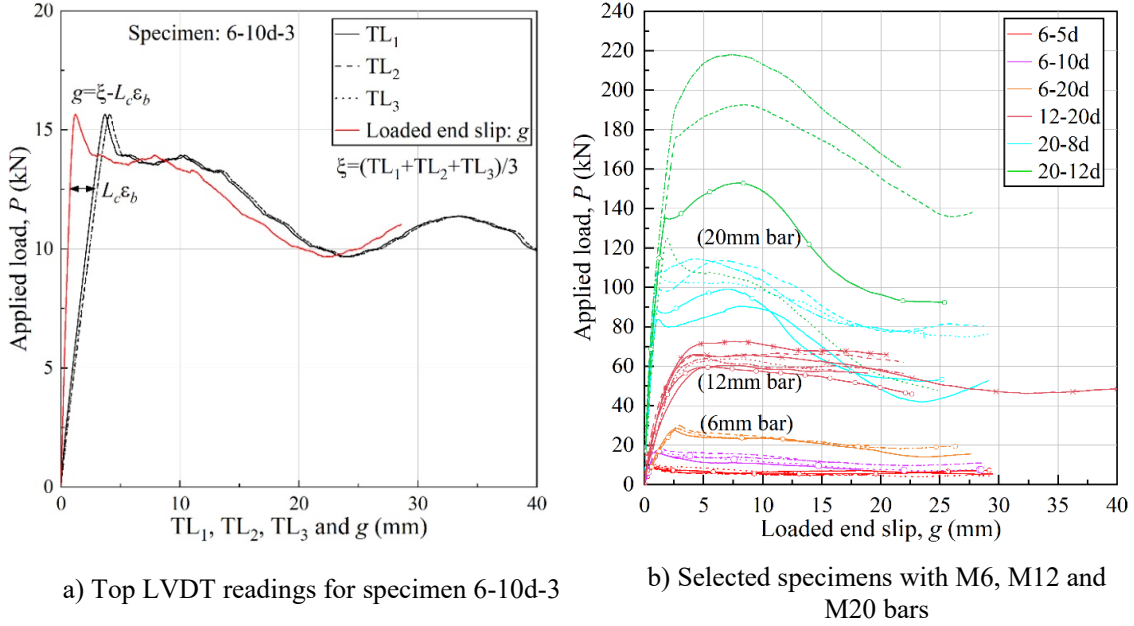


Figure 4: Applied load P versus loaded end slip g responses

Applied load P versus free end slip δ responses.

Figure 5a shows the applied load versus the separate readings of the two bottom LVDTs for a representative M20 specimen (20-8d-3), indicating the consistency of the two responses. In the specimens tested in LVDT control, the bottom LVDTs (BL₁ and BL₂) were installed to measure the free end slip (δ), which corresponds to the average of BL₁ and BL₂ LVDT readings. Figure 5b-d display the applied load (P) versus free end slip (δ) plots for specimens where δ was measured. Figure 5b includes specimens with M6 and M20 bars, Figure 5c includes specimens with M6 and M12 bars, and Figure 5d includes specimens with M12 and M20 bars. A call-out plot within Figure 5c and d focuses on the beginning of the responses. After the initial vertical branch, which represents zero slip at the free end, the P - δ responses exhibit a nonlinear behavior that continues until the peak load is reached.

One interesting observation is that the value of δ corresponding to the peak load is higher for M12 specimens compared to the M6 with the same bonded length, which corresponds to comparing 6-10d and 12-5d specimens (Figure 5c). Further, even when the same bonded area is considered for M6 and M12 specimens, which corresponds to comparing 6-20d and 12-5d specimens, δ corresponding to the peak load is higher for M12 specimens. A similar observation can be made when M12 specimens are compared to the M20 specimens with the same bonded length, which corresponds to comparing 12-20d and 20-12d specimens (Figure 5d), i.e., the free end slip of M20 specimens at the peak load is higher than that of M12 specimens. In terms of same bonded area, an exact match between M12 and

M20 specimens cannot be found, however, the comparison between δ corresponding to the peak load for 20-8d and 12-20d specimens indicates a similar behavior as above.

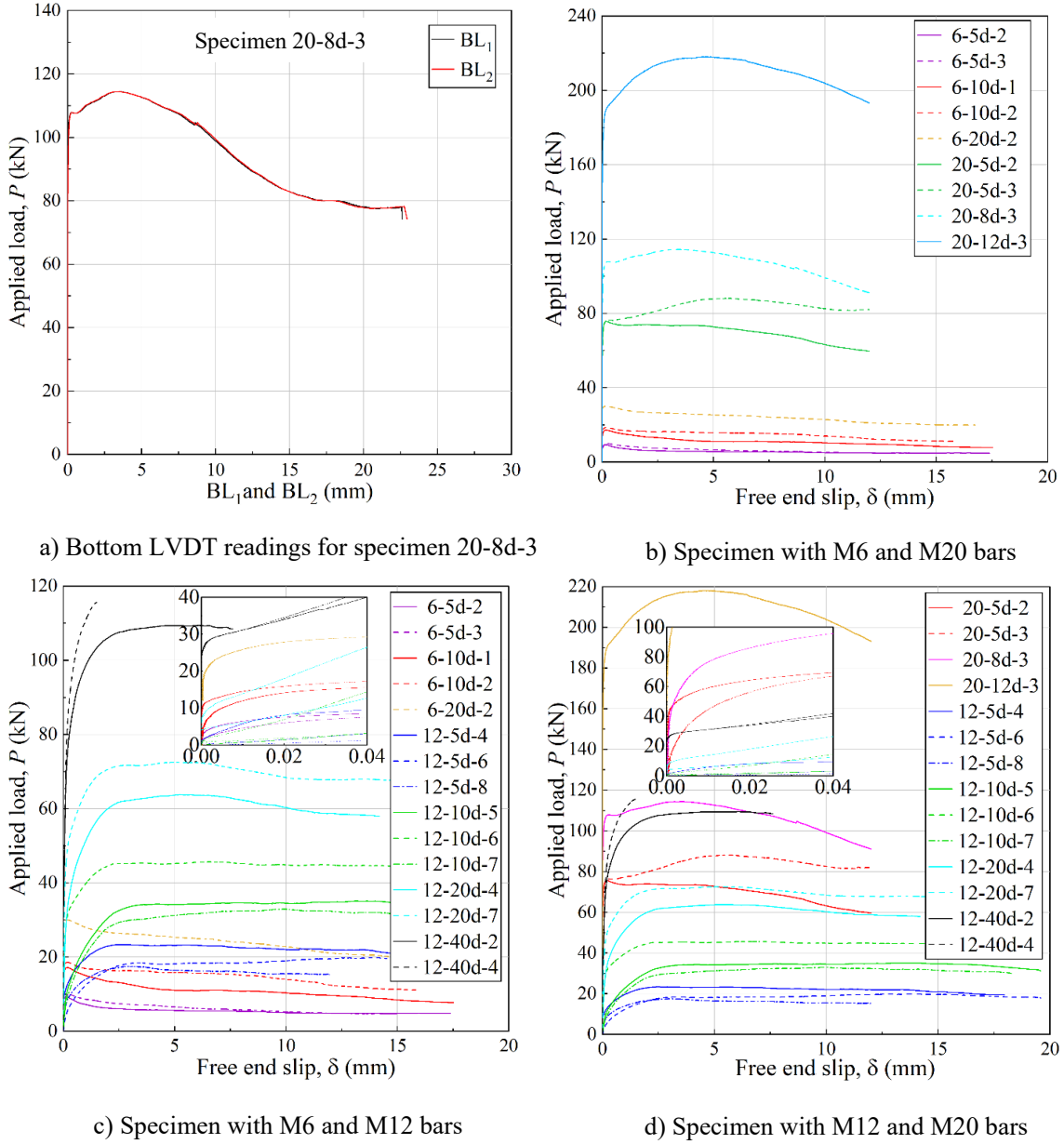


Figure 5: Applied load P versus free end slip δ responses.

Effect of bar diameter on the bond behavior

In Figure 6a-c, the axial stress of the GFRP bar (f_b) is plotted against the machine stroke (t) for specimens with different bar diameters and same bonded lengths.

The axial stress (f_b) is calculated by dividing the applied load (P) by the nominal cross-sectional area ($\pi d_b^2 / 4$) of the GFRP bar:

$$f_b = \frac{4P}{\pi d_b^2} \quad \text{Eq. 1}$$

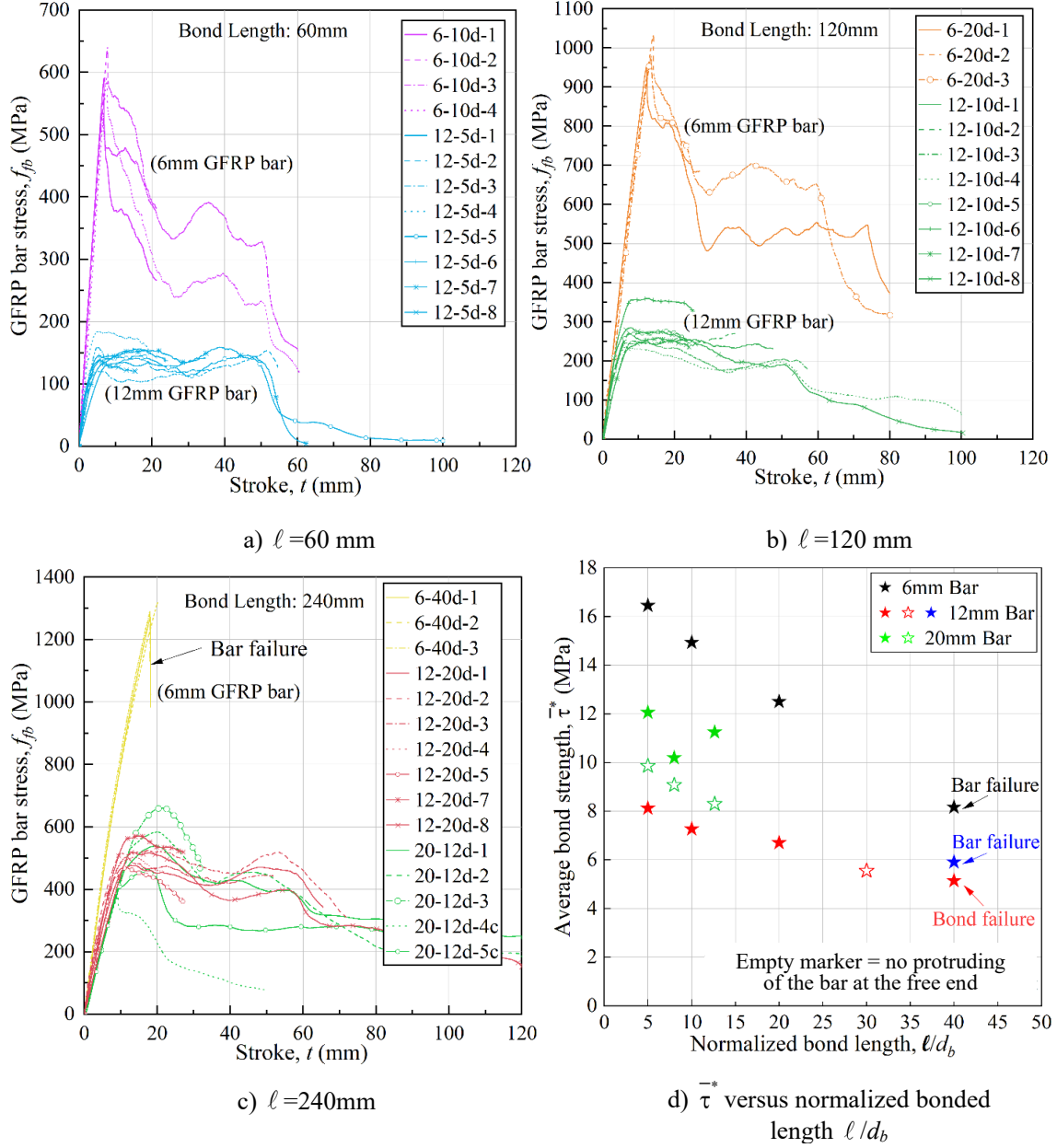


Figure 6: Axial stress of GFRP bar f_{fb} versus stroke t for different bar diameters and average bond strength $\bar{\tau}^*$ versus normalized bond length ℓ/d_b .

In Figure 6a, for a bonded length of 60 mm, the peak axial stress of M6 specimens is approximately 3.8 times higher than that of M12 specimens. Similarly, in Figure 6b, for a bonded length of 120 mm, the peak axial stress of M6 specimens is approximately 3.5 times higher than that of M12 specimens. For the specimens with a bonded length of 240 mm (Figure 6c), the M6 bars reached failure at the peak stress. The difference in behavior between M6 and M12 bars with the same bonded length suggests that the axial stress distribution in the bar is influenced by the bar size. In Figure 6c, it is observed that the specimens with M20 bars exhibit a similar peak axial stress to the M12 bar specimens with the same bonded length of 240 mm. Further analysis will be necessary to understand the behavior of M20 bars.

In Figure 6d, the average bond strength is plotted against the normalized bonded length (ℓ/d_b) for different bar diameters. The average bond strength $\bar{\tau}^*$ is calculated by dividing the average peak

applied load \bar{P}^* (for specimens with the same bar diameter and bonded length) by the bonded area $\pi d_b \ell$:

$$\bar{\tau}^* = \frac{\bar{P}^*}{\pi d_b \ell} \quad \text{Eq. 2}$$

The analysis of the average bond strength versus normalized bonded length for different bar diameters reveals interesting trends. For the M6 bar specimens, there is an almost linear decrease in average bond strength as the bonded length increases for the first three lengths. However, it should be noted that for the fourth bonded length ($\ell = 240$ mm), the bar failed in tension at the peak load, indicating that if failure had not occurred, the average bond strength could have reached even higher values. M12 bar specimens show a non-linear trend in average bond strength versus bonded length. The overall average bond strength for M12 bars is lower than that of M6 bars. In the case of M20 bar specimens, the trend in average bond strength versus bonded length is different from that of M12 bars. When the specimens feature the protruding part of the bar at the free end, the bond strength initially decreases from the first to the second bonded length, but then increases from the second to the third bonded length. This unique trend requires further investigation for the M20 bars as mentioned above. In addition, a decreasing trend can be observed for M20 bars when the protruding part of the bar was cut off.

It is important to note that the concrete compression strength at 28 days for M6 and M20 versus M12 bar specimens were slightly different (41.6 MPa and 34.0 MPa, respectively). However, in this study, the effect of the concrete strength was ignored as all the specimens experienced pull-out failure on the external layer of the bar. The previous study published by the authors (Zhao et al., 2022) showed that for this specific sand coated bar, slippage of the bar was associated with grooving of the surface of the bar caused by the sand that remained attached to the concrete bulk.

CONCLUSIONS

Based on the experimental results and discussions in the paper, the following conclusions can be drawn regarding the bond behavior of the different bar diameters (6mm, 12mm, and 20mm):

- 1) The measurements of elastic modulus revealed that larger bar diameters exhibited lower elastic modulus values compared to smaller bar diameters.
- 2) Similar bond behavior was found for all the different bar diameters (M6, M12, and M20) for this type of sand coated and carbon fiber wrapped GFRP bars.
- 3) The axial stress at peak load of the smaller diameter bars was found to be higher compared to the larger diameter bars.
- 4) The average bond strength decreased as the bar diameter increased for the same bonded length. However, additional work is needed to assess the reason why the M20 bars did not follow the trend exhibited by the M6 and M12 bars.

ACKNOWLEDGEMENT

The authors gratefully acknowledge Mr. Michael Butler, Engineer in the Concrete Laboratory at Case Western Reserve University. Sireg Geotech S.r.l. is also acknowledged for providing the GFRP bars. Drs. D'Antino and Focacci acknowledge the support of the DPC-ReLUIIS 2022–2024 project (WP 14) funded by the Italian Department of Civil Protection. Dr. Carloni acknowledges the support of ACI CRC 2022 grant #P0060 and from grant RES515729 from National Center for Transportation (Washington State University).

CONFLICT OF INTEREST

The authors declare that they have no conflicts of interest associated with the work presented in this paper.

DATA AVAILABILITY

Data on which this paper is based is available from the authors upon reasonable request.

REFERENCES

- Achillides, Z., & Pilakoutas, K. (2004). Bond Behavior of Fiber Reinforced Polymer Bars under Direct Pullout Conditions. *Journal of Composites for Construction*, 8(2), 173–181.
[https://doi.org/10.1061/\(ASCE\)1090-0268\(2004\)8:2\(173\)](https://doi.org/10.1061/(ASCE)1090-0268(2004)8:2(173))
- ACI 440 (Ed.). (2012). *440.3R-12—Guide test methods for fiber-reinforced polymers (FRPs) for reinforcing or strengthening concrete and masonry structures* (1. print). American Concrete Institute.
- Ali, A. H., Mohamed, H. M., & Benmokrane, B. (2020). Bar size effect on long-term durability of sand-coated basalt-FRP composite bars. *Composites Part B: Engineering*, 195, 108059.
<https://doi.org/10.1016/j.compositesb.2020.108059>
- Arias, J. P. M., Vazquez, A., & Escobar, M. M. (2012). Use of sand coating to improve bonding between GFRP bars and concrete. *Journal of Composite Materials*, 46(18), 2271–2278.
<https://doi.org/10.1177/0021998311431994>
- ASTM C09. (2020a). *ASTM C39/C39M-21—Standard Test Method for Compressive Strength of Cylindrical Concrete Specimens*. ASTM International.
https://doi.org/10.1520/C0039_C0039M-20
- ASTM C09. (2020b). *C143/C143M – 20—Standard Test Method for Slump of Hydraulic-Cement Concrete*. ASTM International. https://doi.org/10.1520/C0143_C0143M-20
- ASTM D30. (2020). *ASTM D7913/D7913M-14. Standard Test Method for Bond Strength of Fiber-Reinforced Polymer Matrix Composite Bars to Concrete by Pullout Testing*.
https://www.astm.org/d7913_d7913m-14.html
- ASTM D30. (2021). *D7205/D7205M-21—Standard Test Method for Tensile Properties of Fiber Reinforced Polymer Matrix Composite Bars*.
<https://standards.globalspec.com/std/10056396/astm-d7205-d7205m>
- ASTM International. (2016). *Standard Test Method for Tensile Properties of Fiber Reinforced Polymer Matrix Composite Bars. ASTM D7205/D7205M - 06*.
https://www.astm.org/d7205_d7205m-06.html
- Baena, M., Torres, L., Turon, A., & Barris, C. (2009). Experimental study of bond behaviour between concrete and FRP bars using a pull-out test. *Composites Part B: Engineering*, 40(8), 784–797.
<https://doi.org/10.1016/j.compositesb.2009.07.003>
- C. Arya, C., Clarke, J. L., Kay, E. A., & O'Regan, P. D. (2012). *Design guidance for strengthening concrete structures using fibre composite materials: Report of a Concrete Society Working Party* (Third edition). Concrete Society.
- CSA. (2021). *Design and construction of building structures with fibre-reinforced polymers* (CAN/CSA S806-12). <https://webstore.ansi.org/Standards/CSA/csas80612>
- El Refai, A., Ammar, M.-A., & Masmoudi, R. (2015). Bond Performance of Basalt Fiber-Reinforced Polymer Bars to Concrete. *Journal of Composites for Construction*, 19(3), 04014050.
[https://doi.org/10.1061/\(ASCE\)CC.1943-5614.0000487](https://doi.org/10.1061/(ASCE)CC.1943-5614.0000487)
- El-Hacha, R., Cheng, L. (Dawn), Lopez de Murphy, M., & Gold, W. J. (Eds.). (1993). *Fiber-Reinforced-Plastic Reinforcement for Concrete Structures—13th International Symposium*. American Concrete Institute.
- Fib, C. J. (2007). *fib Bulletin 40. FRP reinforcement in RC structures* (fib. The International Federation for Structural Concrete, Ed.). fib. The International Federation for Structural Concrete. <https://doi.org/10.35789/fib.BULL.0040>
- Hu, X., Xiao, J., Zhang, K., & Zhang, Q. (2022). The state-of-the-art study on durability of FRP reinforced concrete with seawater and sea sand. *Journal of Building Engineering*, 51, 104294.
<https://doi.org/10.1016/j.job.2022.104294>
- Huang, L., Chen, J., Qu, J., & Dai, Q. (2020). Modeling for bond-constitutive relationships of FRP rebars to concrete matrix. *Construction and Building Materials*, 263, 120654.
<https://doi.org/10.1016/j.conbuildmat.2020.120654>
- ISO. (2015). *Fibre-reinforced polymer (FRP) reinforcement of concrete—Test methods*. ISO.
<https://www.iso.org/cms/render/live/en/sites/isoorg/contents/data/standard/06/36/63657.html>

- Junyan, D., Shiping, Y., & Changshun, H. (2021). Analysis of key influencing factors of the bond performance between BFRP bars and coral reef and sand concrete. *Construction and Building Materials*, 269. <https://doi.org/10.1016/j.conbuildmat.2020.121248>
- Okelo, R., & Yuan, R. L. (2004). Realistic Bond Strength of FRF Rebars in NSC from Beam Specimens. *Engineering Construction and Operations in Challenging Environments Earth and Space 2004: Proceedings of the Ninth Biennial ASCE Aerospace Division International Conference*, 20(3), 609–616. [https://doi.org/10.1061/\(asce\)0893-1321\(2007\)20:3\(133\)](https://doi.org/10.1061/(asce)0893-1321(2007)20:3(133))
- Rolland, A., Quiertant, M., Khadour, A., Chataigner, S., Benzarti, K., & Argoul, P. (2018). Experimental investigations on the bond behavior between concrete and FRP reinforcing bars. *Construction and Building Materials*, 173, 136–148. <https://doi.org/10.1016/j.conbuildmat.2018.03.169>
- Sayed Ahmad, F., Foret, G., & Le Roy, R. (2011). Bond between carbon fibre-reinforced polymer (CFRP) bars and ultra high performance fibre reinforced concrete (UHPFRC): Experimental study. *Construction and Building Materials*, 25(2), 479–485. <https://doi.org/10.1016/j.conbuildmat.2010.02.006>
- Shen, D., Shi, X., Zhang, H., Duan, X., & Jiang, G. (2016). Experimental study of early-age bond behavior between high strength concrete and steel bars using a pull-out test. *Construction and Building Materials*, 113, 653–663. <https://doi.org/10.1016/j.conbuildmat.2016.03.094>
- Sireg Geotech S r. l. (2017). *Glasspreet Technical Data Sheet (provided privately by the manufacturer)*. Provided privately by the manufacturer. Provided privately by the manufacturer
- Tighiouart, B., Benmokrane, B., & Gao, D. (1998). *Investigation of bond in concrete member with fibre reinforced polymer (FRP) bars*. 10.
- Wei, W., Liu, F., Xiong, Z., Lu, Z., & Li, L. (2019). Bond performance between fibre-reinforced polymer bars and concrete under pull-out tests. *Construction and Building Materials*, 227, 116803. <https://doi.org/10.1016/j.conbuildmat.2019.116803>
- Zhao, X., Minhajur Rahman, M., D'Antino, T., Focacci, F., & Carloni, C. (2022). Effect of bonded length on the load response and failure mode of pull-out tests of GFRP bars embedded in concrete. *Construction and Building Materials*, 347, 128425. <https://doi.org/10.1016/j.conbuildmat.2022.128425>